Received: 22 July 2022 | Revised: 11 November 2022 | Accepted: 19 December 2022

DOI: 10.1111/gbi.12543

ORIGINAL ARTICLE

gebiology WILEY

Effects of RuBisCO and CO_2 concentration on cyanobacterial growth and carbon isotope fractionation

Amanda K. Garcia[1] | Mateusz Kędzior[1] | Arnaud Taton[2] | Meng Li[3] | Jodi N. Young[3] | Betül Kaçar[1]

[1]Department of Bacteriology, University of Wisconsin – Madison, Madison, Wisconsin, USA

[2]Division of Biological Sciences, University of California San Diego, La Jolla, California, USA

[3]School of Oceanography, University of Washington, Seattle, Washington, USA

Correspondence
Department of Bacteriology, University of Wisconsin – Madison, Madison, WI, USA.
Email: bkacar@wisc.edu

Funding information
National Aeronautics and Space Administration; National Institutes of Health; National Science Foundation; Simons Foundation

Abstract

Carbon isotope biosignatures preserved in the Precambrian geologic record are primarily interpreted to reflect ancient cyanobacterial carbon fixation catalyzed by Form I RuBisCO enzymes. The average range of isotopic biosignatures generally follows that produced by extant cyanobacteria. However, this observation is difficult to reconcile with several environmental (e.g., temperature, pH, and CO_2 concentrations), molecular, and physiological factors that likely would have differed during the Precambrian and can produce fractionation variability in contemporary organisms that meets or exceeds that observed in the geologic record. To test a specific range of genetic and environmental factors that may impact ancient carbon isotope biosignatures, we engineered a mutant strain of the model cyanobacterium *Synechococcus elongatus* PCC 7942 that overexpresses RuBisCO across varying atmospheric CO_2 concentrations. We hypothesized that changes in RuBisCO expression would impact the net rates of intracellular CO_2 fixation versus CO_2 supply, and thus whole-cell carbon isotope discrimination. In particular, we investigated the impacts of RuBisCO overexpression under changing CO_2 concentrations on both carbon isotope biosignatures and cyanobacterial physiology, including cell growth and oxygen evolution rates. We found that an increased pool of active RuBisCO does not significantly affect the $^{13}C/^{12}C$ isotopic discrimination (ε_p) at all tested CO_2 concentrations, yielding ε_p of ≈ 23‰ for both wild-type and mutant strains at elevated CO_2. We therefore suggest that expected variation in cyanobacterial RuBisCO expression patterns should not confound carbon isotope biosignature interpretation. A deeper understanding of environmental, evolutionary, and intracellular factors that impact cyanobacterial physiology and isotope discrimination is crucial for reconciling microbially driven carbon biosignatures with those preserved in the geologic record.

KEYWORDS
biosignatures, carbon fixation, carbon isotope fractionation, cyanobacteria, RuBisCO

1 | INTRODUCTION

The conserved microbial metabolic pathways that drive global biogeochemistry emerged on Earth billions of years ago, the evolution of which has both shaped and been shaped by large-scale environmental transitions (Falkowski et al., 2008; Knoll & Nowak, 2017; Lyons et al., 2015). These microbial processes have left distinct signatures that are evidence of biological activity billions of years in the past. The oldest and most extensive signature of biological activity on Earth is the deviation in stable carbon isotopic compositions ($^{13}C/^{12}C$, expressed as $\delta^{13}C$) between preserved inorganic and organic carbon, interpreted to reflect the isotopic discrimination of ancient biological carbon fixation (Des Marais, 2001; Krissansen-Totton et al., 2015; Lloyd et al., 2020; Schidlowski, 2001). This deviation is primarily shaped by enzymes that preferentially assimilate the lighter ^{12}C isotope from inorganic carbon sources. Carbon biosignatures preserved in the geologic record therefore reflect the long-term evolution of these enzyme-mediated processes and their hosts' physiologies.

The RuBisCO enzyme (ribulose 1,5-bisphosphate (RuBP) carboxylase/oxygenase) catalyzes the reduction in inorganic CO_2 as the initial step of carbon assimilation into organic biomass via the Calvin–Benson–Bassham (CBB) cycle (Erb & Zarzycki, 2018; Nisbet et al., 2007; Tcherkez et al., 2006). RuBisCO is one of the most abundant proteins on Earth (Bar-On & Milo, 2019; Ellis, 1979; Raven, 2013), and its presence in photoautotrophic organisms, including early-evolved cyanobacteria, suggests that this enzyme has played a significant role in primary production for much of Earth history (Hamilton et al., 2016; Schirrmeister et al., 2016; Schopf, 2011). Thus, the isotopic fractionation behavior of RuBisCO is also thought to have largely influenced Precambrian carbon isotope signatures preserved in the geologic record (Garcia et al., 2021; Schidlowski, 1988). Although there are multiple forms of RuBisCO, the known range of the Form IA/IB RuBisCO isotopic effect ($\varepsilon \approx 20‰–30‰$) (Guy et al., 1993; Scott et al., 2007; von Caemmerer et al., 2014)—the form utilized by extant cyanobacteria and responsible for the bulk of modern primary production (Field, 1998)—is largely consistent with the ~25‰ mean deviation between preserved inorganic and organic carbon isotopic compositions across geologic time (Des Marais, 2001; Havig et al., 2017; Kedzior et al., 2022; Krissansen-Totton et al., 2015; Lloyd et al., 2020; Schidlowski, 2001). The kinetic isotopic effects of cyanobacterial Form IA and IB RuBisCOs in particular have been measured between ~22‰ and 24‰ (Guy et al., 1993; Scott et al., 2007), whereas land plant Form IB RuBisCOs typically have larger effects of up to ~29‰ (von Caemmerer et al., 2014) and Form ID RuBisCOs have exhibited smaller effects between ~11‰ and 19‰ when measured in vitro (Boller et al., 2011, 2015), though in vivo assays of red algal Form ID RuBisCOs indicate much larger values (MacFarlane & Raven, 1990; Stepien & Austin, 2015).

RuBisCO is an important factor in the generation of distinct carbon isotopic biosignatures associated with CBB-utilizing organisms (Hayes, 2001; Laws et al., 1995; Wilkes & Pearson, 2019). Nonetheless, the carbon isotopic composition of bulk photoautotrophic biomass often deviates from values obtained for purified RuBisCOs, a discrepancy at least partially explained by the fact that the latter are measured at CO_2 saturation (e.g., (Boller et al., 2011; Guy et al., 1993; Scott et al., 2007; von Caemmerer et al., 2014)). This discrepancy might also be attributable to several intracellular physiological and metabolic features that additionally shift the isotopic composition in organism biomass. These include the activity of carbon-concentrating mechanisms (CCM) that elevate CO_2 in RuBisCO-containing cellular compartments (Hurley et al., 2021; Laws et al., 2002; Price et al., 2008; Raven et al., 2008; Wilkes & Pearson, 2019) and the diffusive transport of CO_2 (Hayes, 1993; Rau et al., 1996). Studies have shown that photosynthetic carbon isotope discrimination (ε_p) may vary due to environmental factors and cellular physiological responses, including temperature (Deleens et al., 1985; Wong & Sackett, 1978), pH (Hinga et al., 1994; Roeske & O'Leary, 1984), growth rate (Bidigare et al., 1997; Laws et al., 1997), and CO_2 concentration (Eichner et al., 2015; Freeman & Hayes, 1992; Hinga et al., 1994; Hurley et al., 2021; Schubert & Jahren, 2012; Wilkes et al., 2018), as well as light, nutrient, and water availability (Cernusak et al., 2013; Eek et al., 1999; Hill et al., 2008).

An aspect of photoautotrophic carbon isotopic discrimination that has not been thoroughly investigated is how varying RuBisCO expression may have influenced ancient host organism growth and biosignature generation. Evolutionary biologists have long debated the role of genetic regulation versus protein-level variation in evolutionary selection (Carroll, 2005; Fay & Wittkopp, 2008; Olson-Manning et al., 2012; Taylor et al., 2022; Wilson et al., 1974). Whereas catalytic properties of proteins may diverge according to their specific amino-acid compositions and structures, their overlying genetic regulation (i.e., controls on the timing, regulation and magnitude of protein expression) can additionally affect observed metabolic outputs of interest to geobiologists. The evolution of genetic regulation is often overlooked in geobiological evaluation of ancient microbial biosignatures due to the challenges involved with disentangling their effects from other variables. For carbon isotope discrimination in particular, the cellular quantity of RuBisCO might impact to what degree the RuBisCO kinetic isotope effect is expressed by influencing the rate of CO_2 consumption compared with rate of CO_2 supply.

RuBisCO expression has been shown to be CO_2-sensitive (Gesch et al., 2003; Onizuka et al., 2002; Sengupta et al., 2019). This observation is particularly important, considering that atmospheric CO_2 concentrations exceeded present-day levels by more than an order of magnitude for much of Earth history (between ~0.001 and 0.1 bar CO_2 through the Precambrian (Catling & Zahnle, 2020)) and that ancient RuBisCOs likely navigated a tradeoff between carboxylase turnover rates and CO_2/O_2 selectivity to adapt to varying historical CO_2/O_2 levels (Erb & Zarzycki, 2018; Kacar et al., 2017; Poudel et al., 2020; Tcherkez et al., 2006). Although both in vivo and in vitro experimental work has demonstrated the positive correlation between CO_2 levels and RuBisCO isotopic discrimination (Freeman & Hayes, 1992; Hinga et al., 1994; Schubert & Jahren, 2012; Wilkes et al., 2018), the role

of RuBisCO expression, given its CO_2 sensitivity, has not yet been explored. Furthermore, quantifying the biosignature-level impacts of RuBisCO expression would improve interpretation of experimental studies that characterize the carbon isotopic discrimination of environmentally or genetically perturbed laboratory models, as these perturbations are likely to generate RuBisCO expression variability.

To investigate the interplay between RuBisCO expression and CO_2 concentration as well as their effects on cyanobacterial physiology and carbon isotopic discrimination, we generated a genetic system to manipulate the expression levels of RuBisCO in the model organism *Synechococcus elongatus* PCC 7942 (hereafter *S. elongatus*) (Bonfil et al., 1998; Gabay et al., 1998; Maeda et al., 2000; Omata et al., 2001; Tchernov et al., 2001). Genetic engineering is facilitated by this strain's ability to take up and integrate exogenous DNA into its genome by homologous recombination (Taton et al., 2020). *S. elongatus* also possesses the β-carboxysome-based CCM that likely impacted the production of Precambrian carbon biosignatures following the rise of atmospheric oxygen (Hurley et al., 2021; Lyons et al., 2014). Thus, *S. elongatus* is a suitable model to study the genetic basis of ancient carbon biosignatures. We engineered its genome with an additional copy of the RuBisCO operon and confirmed overexpression of RuBisCO under both ambient and elevated CO_2 levels. Then, we determined growth rate, photosynthetic oxygen evolution rate, and $^{13}C/^{12}C$ discrimination of the engineered strain in comparison to wild-type *S. elongatus* under different atmospheric conditions.

2 | RESULTS

2.1 | A second copy of the *rbc* operon results in increased amount of active RuBisCO

The RuBisCO Form IB enzyme in *S. elongatus* is encoded by an operon that includes a CO_2-sensitive promoter region (Sengupta et al., 2019) and the structural *rbcL* (large subunit) and *rbcS* (small subunit) genes (Vijayan et al., 2011). We designed *S. elongatus* strain Syn02 that harbors the native *rbc* operon and a second copy inserted in the chromosome neutral site 2 (NS2), a site that permits genetic modification without additional indirect phenotypic impact (Andersson et al., 2000; Clerico et al., 2007) (Figure 1). Additionally, we generated a control strain (Syn01) whereby RuBisCO is provided solely by an engineered *rbc* operon at its NS2 site (Table 1). Attributes of these strains related to carbon fixation, including RuBisCO transcription and protein expression, carboxylase activity, and carbon isotope fractionation, were evaluated under different CO_2 conditions, including ambient (~0.04%), 2%, and 5% CO_2 concentrations. These CO_2 concentrations were selected to measure the impact of a Precambrian-like atmosphere, which is generally constrained between ~0.1% and ~10% CO_2 for much of the early evolution of cyanobacteria (assuming ~1-bar total paleopressure) (Catling & Zahnle, 2020).

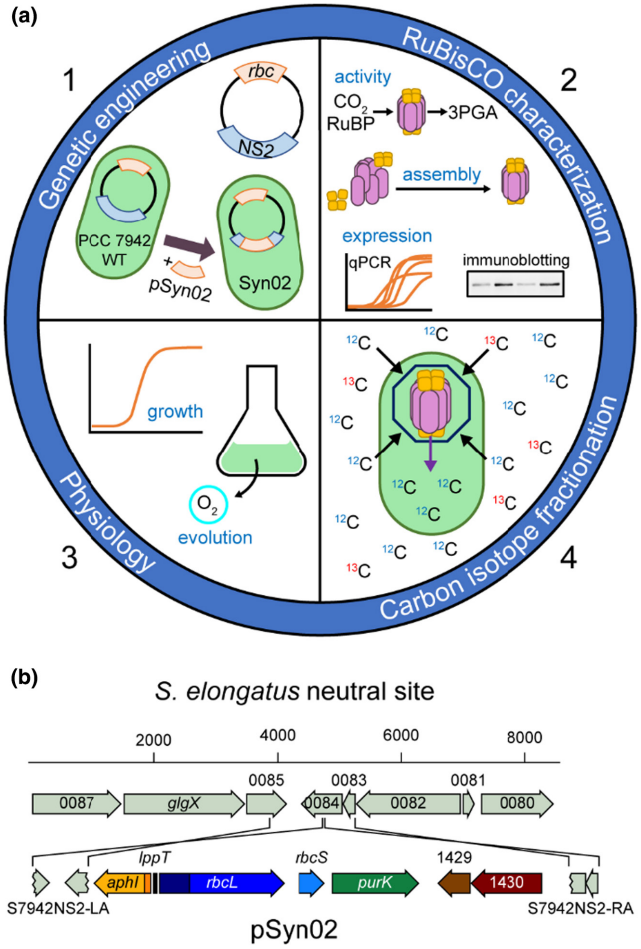

FIGURE 1 Experimental strategy. (a) Overall methodology. (1) Genetic engineering: An additional copy of the *rbc* operon was inserted at the chromosomal NS2 site of *S. elongatus* PCC 7942 to create the Syn02 strain. (2) RuBisCO characterization: Protein-level analysis was carried out by investigating catalytic activity, assembly into a hexadecameric complex, and expression at both the transcript and protein levels. (3) Physiology: *S. elongatus* WT and Syn02 strains were evaluated by monitoring microbial growth characteristics and rate of photosynthetic oxygen evolution. (4) Carbon isotope fractionation: The impact of RuBisCO overexpression on biomass $\delta^{13}C$ under varying CO_2 concentrations was assessed. (b) Map of the genetic insert in *S. elongatus* strain Syn02. Plasmid pSyn02 was used to insert the *rbc* operon and the *aph1* gene conferring kanamycin resistance in PCC 7942 WT NS2 to generate the Syn02 strain. Crosslines indicate homologous recombination sites and scale bars show DNA fragment sizes (in bp).

We evaluated whether the additional copy of the *rbc* operon in strain Syn02 resulted in increased RuBisCO *rbcL* and *purK* (located downstream of *rbcL* in the operon) transcription under varying CO_2 levels (ambient, 2%, and 5% CO_2). Transcription was measured by quantitative reverse-transcription PCR (RT-qPCR), normalized to *secA* and *ppc* reference genes (Hood et al., 2016; Luo et al., 2019; Szekeres et al., 2014). We observed that elevated CO_2 enhanced WT *rbcL* transcription by at least ~5-fold relative to ambient conditions ($p < .001$; Figure 2b, Figure S1B; see Materials and Methods). *rbcL*

TABLE 1 Strains and plasmids used in this study

Strain or plasmid	Description/genotype	Antibiotic resistance	Source/reference
WT	Wild-type strain of *S. elongatus* PCC 7942	-	Susan S. Golden (UC San Diego)
pAM4937	Expression vector for *S. elongatus* PCC 7942 neutral site 2 (NS2)	Km	(Taton et al., 2014)
pSyn02	pAM4937 carrying the *rbc* operon including *rbcL*, *rbcS*, *purK*, and flanking sequences from *S. elongatus* PCC 7942 (CP000100: 1,479,071–1,484,283)	Km	This study
Syn02	*S. elongatus* PCC 7942 carrying a second copy of the *rbc* operon and flanking sequences at NS2: NS2::*aphI-rbcL-rbcS-purK*- Synpcc7942_1429- Synpcc7942_1430	Km	This study
pAM4951	Expression vector for *S. elongatus* PCC 7942 neutral site 1 (NS1)	Sp + Sm	(Taton et al., 2014)
pSyn01	Plasmid to replace *S. elongatus'* native *rbc* operon (CP000100: 1,479,070–1,482,595) with a Sp/Sm resistance gene: Δ(*rbcL-rbcS-purK*)::*aadA*.	Sp + Sm	This study
Syn01	*S. elongatus* strain Syn02 with the native *rbc* operon removed: Syn02 and and Δ(*rbcL-rbcS-purK*)::*aadA*.	Km, Sp + Sm	This study

transcription was further increased by at least ~2-fold in Syn02 relative to WT across all tested CO_2 levels and growth phases, and as high as ~14-fold in air ($p < .01$; Figure 2a, Figure S1A). Expression of *purK* in Syn02 increased by >2-fold at 2% and 5% CO_2 relative to WT, but decreased by ~0.5-fold in air (Figure S1C).

To determine RuBisCO overexpression at the protein-level, we quantified RbcL protein from crude cell lysates by Western blot using rabbit anti-RbcL antibody (see Materials and Methods). In agreement with RuBisCO overexpression indicated by the RT-qPCR results, densitometric analyses revealed a mean ~2 to 4-fold increase of RbcL protein in Syn02 relative to WT across all tested CO_2 concentrations ($p < .01$; Figure 2c). Finally, we confirmed proper assembly of the large (L) and small (S) subunits into the RuBisCO L_8S_8 complex in Syn02 as well as the Syn01 control strain by native protein electrophoresis and detection by anti-RbcL antibody. At 2% CO_2, we found a ~3-fold increase in assembled RuBisCO protein for Syn02 and ~2-fold increase for Syn01 relative to WT for cultures grown in 2% CO_2 (Figure 2d).

Finally, we tested whether RuBisCO overexpression in Syn02 resulted in an increased amount of active RuBisCO by determining the total carboxylase activity of cell lysates. Because we detected the smallest increase in transcript levels for Syn02 relative to WT under 2% CO_2, we selected this growth condition to provide a reasonable lower bound on Syn02 RuBisCO activity. We measured a mean ~1.8-fold ($p < .01$) increase in Syn02 lysate RuBisCO activity relative to WT (Figure 2e). Despite the modest increase in assembled RuBisCO detected for the control strain, Syn01, no significant difference in activity was found between Syn01 and WT cultures grown in these same conditions.

2.2 | RuBisCO overexpression does not strongly influence growth rate or photosynthetic activity

Following confirmation that Syn02 overexpresses active RuBisCO, we compared growth rates of WT and Syn02 *S. elongatus* strains at different CO_2 levels to identify potential downstream physiological effects of increased RuBisCO protein. WT and Syn02 both exhibited ~2.5-fold faster growth rates under 2% and 5% CO_2 compared with ambient air ($p < .001$; Figure 3; Table 2). Syn02 exhibited a slight ~1.1-fold increase in growth rate in ambient air relative to WT ($p < .05$). No difference in growth rate was observed between the two strains under 2% and 5% CO_2. The carrying capacity (maximum cell density measured at OD_{750} across the total growth period) for cultures varied between different atmospheric conditions, with a maximum carrying capacity of $OD_{750} \approx 8.4$ reached under 2% CO_2. No significant difference in carrying capacity was found between WT and Syn02 cultures grown under the same atmospheric conditions. These experiments were replicated with unsparged cultures, yielding consistent results (Table S1).

To further test for differences in photosynthetic activities between the WT and Syn02 strains, we measured their oxygen evolution rates in ambient air. After brief incubation in the dark, culture samples were exposed to saturated light in an oxygen electrode chamber to detect levels of molecular oxygen. Oxygen evolution rates were normalized to chlorophyll *a* concentrations, following Zavřel et al. (2015). We did not observe a significant difference in mean oxygen evolution rate between WT and Syn02 (340 ± 30 $O_2 \cdot h^{-1} \cdot \mu g^{-1}$ chlorophyll *a* and 360 ± 30 $O_2 \cdot h^{-1} \cdot \mu g^{-1}$ chlorophyll *a*, respectively) (Table 2).

2.3 | *S. elongatus* $^{13}C/^{12}C$ fractionation is insensitive to RuBisCO overexpression

We tested the combined influence of RuBisCO overexpression and CO_2 concentration on the magnitude of whole-cell $^{13}C/^{12}C$ isotopic discrimination in *S. elongatus*. The isotopic compositions ($\delta^{13}C$) of CO_2 gas ($CO_{2(g)}$) in the headspace, the dissolved inorganic carbon pool (DIC), and biomass, as well as pH of the growth medium, were measured during the early exponential growth phase (pH of growth medium also measured prior to culture inoculation; Supplementary

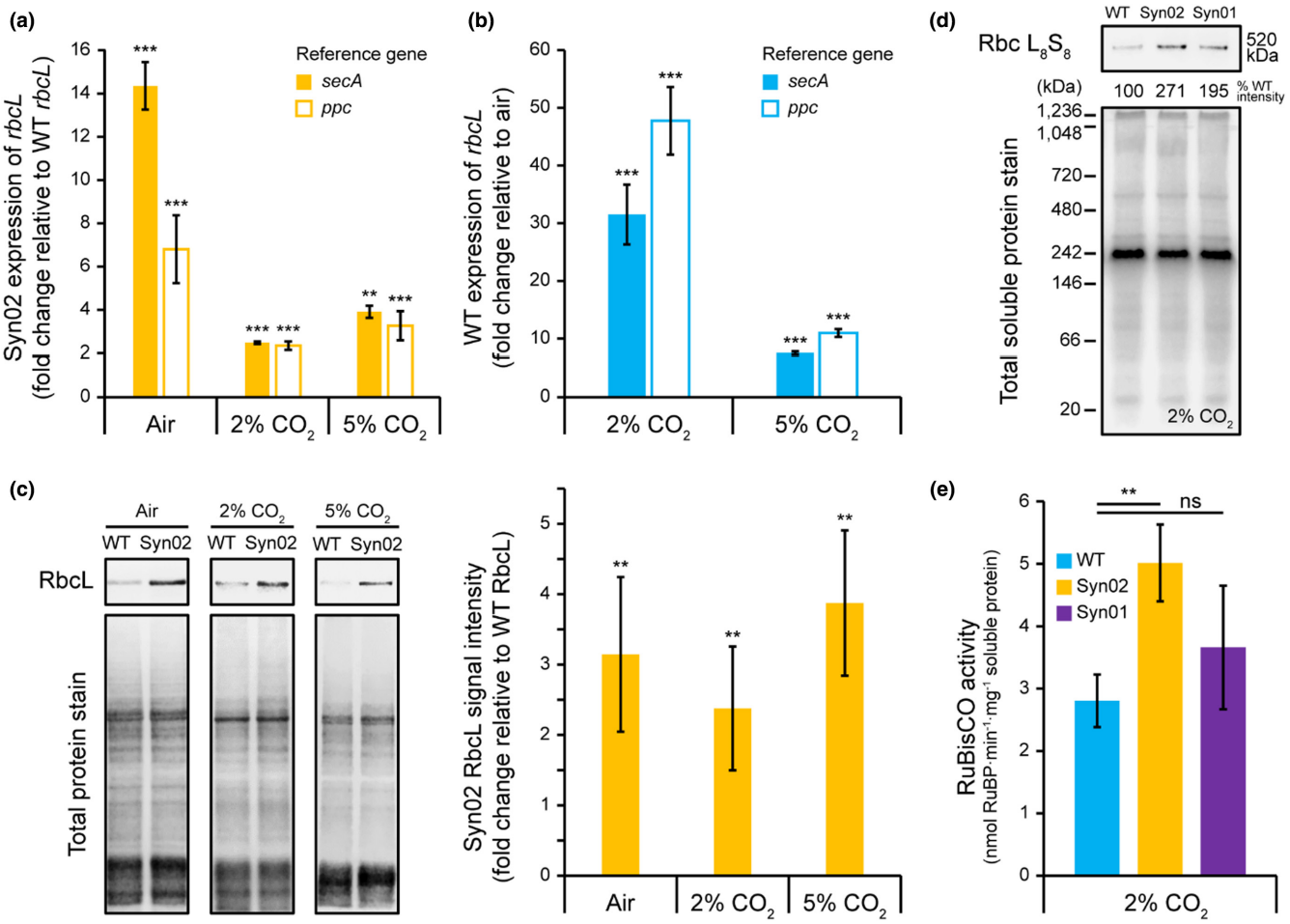

FIGURE 2 RuBisCO expression, assembly, and activity in *S. elongatus* strains under varying CO_2 concentrations. (a) Expression of Syn02 *rbcL* relative to WT *rbcL*. Asterisks indicate *t*-test results compared to WT *rbcL* expression at the same growth condition. (b) Expression of WT *rbcL* at 2% and 5% CO_2 relative to ambient air. Asterisks indicate *t*-test results compared to WT *rbcL* expression in air. (a,b) Expression data was measured by RT-qPCR, normalized to reference genes *secA* and *ppc*. Columns represent mean fold expression for three biological replicates. (c) Immunodetection of RbcL. (*left*) Western blot showing RbcL protein detected by anti-RuBisCO antibody and total protein stain from crude cell lysates. (*right*) RbcL percentage signal intensities were normalized to that for the total soluble protein load. Columns represent mean RbcL intensities for six biological replicates, relative to mean values for WT cultures at the same growth condition. Asterisks indicate *t*-test results compared to WT RbcL. (d) Immunodetection of assembled RuBisCO. Western blot showing the proper assembly of RbcL and RbcS into the L_8S_8 hexadecameric complex L_8S_8 (520 kDa), detected by anti-RbcL antibody. Rbc L_8S_8 percentage signal intensity was normalized to that for the total soluble protein load, and is shown relative to WT. (e) Lysate RuBisCO activity. Activity was measured by the RuBP consumption rate, normalized to total soluble protein content of cell lysate. Columns represent the mean activity of three biological replicates. Asterisks indicate *t*-test results for pairwise comparison indicated by horizontal line. (a-c,e) Error bars on all graphs indicate ±1 SD. Ns, Not significant; $^{**}p<.01$; $^{***}p<.001$.

Information, Table S2 and S3). The difference between source of inorganic carbon ($\delta^{13}C_{CO2(g)}$) and biomass ($\delta^{13}C_{biomass}$), expressed as $\Delta\delta^{13}C_{CO2(g)\text{-}biomass}$ (see Materials and Methods), for WT and Syn02 are shown in Figure 4.

Under ambient conditions, the experimental system was not at equilbirum, with the pH of the culture medium increasing to ~11 between inoculation and isotopic measurement (cyanobacterial mats and blooms have been observed to reach pH > 9 under CO_2 depletion in natural settings (Borovec et al., 2010; Jensen et al., 2011; Wilhelm et al., 2020)). Thus, under these non-equilibrium conditions, $\delta^{13}C$ of aqueous CO_2 ($\delta^{13}CO_{2(aq)}$), and, by extension, ε_p (the difference between $\delta^{13}C_{CO2(aq)}$ and $\delta^{13}C_{biomass}$), could not be calculated. Nevertheless, we observed that both $\delta^{13}{}_{DIC}$ and $\delta^{13}C_{biomass}$ values did not vary widely as a function of the tested *S. elongatus* strain, and there is no significant difference in $\Delta\delta^{13}C_{CO2(g)\text{-}biomass}$ between WT and Syn02 (4.7 ± 0.3‰ and 5.0 ± 0.5‰, respectively; $p>.05$).

Under increased CO_2 concentrations (2% CO_2), the experimental system is close to equibilibrium, with the isotopic difference between DIC and $CO_{2(g)}$ ($\Delta\delta^{13}C_{DIC\text{-}CO2}$) ≈ 8‰. There was no significant difference in $\Delta\delta^{13}C_{CO2(g)\text{-}biomass}$ between WT and Syn02 strains (22.39 ± 0.07‰ and 22.3 ± 0.4‰, respectively; $p>.05$). If we assume equilibrium under 2% CO_2 and estimate $\delta^{13}C_{CO2(aq)}$, ε_p values for WT and Syn02 are also not significantly different (23.0 ± 0.2‰ and 23.6 ± 0.2‰, respectively; see Materials and Methods for

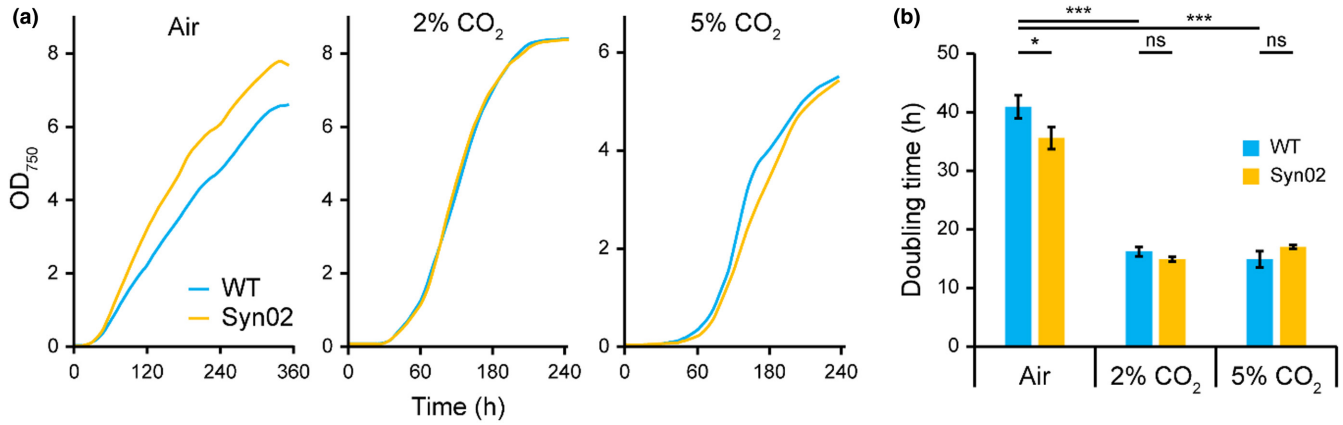

FIGURE 3 Growth of *S. elongatus* strains. (a) Growth profiles. Cultures of each strain were maintained in ambient air or under 2% or 5% CO_2. Smoothed profiles were generated from mean optical density values (measured at 750 nm, OD_{750}) for three replicate cultures per growth condition. (b) Doubling times. Columns represent the mean doubling time of three replicates. Error bars on all graphs indicate ±1 SD, and asterisks indicate *t*-test results for pairwise comparisons indicated by horizontal lines. Ns, Not significant; $^*p<.05$; $^{***}p<.001$

TABLE 2 Growth parameters and oxygen evolution rates of *S. elongatus* strains under varying CO_2 concentrations[a]

Strain	Atmosphere	Growth rate (h^{-1})	Carrying capacity (OD_{750})	Oxygen evolution rate (nmol O_2 h^{-1} μg^{-1} chlorophyll *a*)
WT	Air	0.017 ± 0.001	6.8 ± 0.7	340 ± 30
	2% CO_2	0.043 ± 0.002	8.4 ± 0.5	-
	5% CO_2	0.047 ± 0.005	5.4 ± 0.3	-
Syn02	Air	0.020 ± 0.001*	7.6 ± 0.5	360 ± 30
	2% CO_2	0.046 ± 0.001	8.3 ± 0.2	-
	5% CO_2	0.040 ± 0.001	5.4 ± 0.4	-

[a]Values are means of three biological replicates ±1 SD. Asterisks indicate *t*-test result from comparison with WT for the same atmospheric condition, $^*p<.05$.

calculation). These results demonstrate that the increased RuBisCO transcriptional levels and total carboxylase activity measured for Syn02 in our experiments does not significantly impact whole-cell *S. elongatus* $^{13}C/^{12}C$ discrimination, both at ambient and elevated CO_2 concentrations.

3 | DISCUSSION

In this study, we developed an engineered laboratory system to investigate the coupled impact of elevated CO_2 levels and RuBisCO expression on cyanobacterial physiology and carbon isotope discrimination. We tested whether the overexpression of RuBisCO influences *S. elongatus* growth, photosynthetic oxygen evolution rate, and carbon isotopic signatures at different CO_2 atmosphere concentrations by generating an engineered *S. elongatus* strain Syn02 that harbors a second copy of the *rbc* operon at NS2. We first confirmed overexpression of RuBisCO in our engineered strain, Syn02, by combining transcriptional analyses, protein quantification, and assays of total protein carboxylation activity. Our results show elevated RuBisCO transcription in *S. elongatus* strain Syn02 relative to WT at all tested CO_2 concentrations (ambient air, 2%, and 5% CO_2) (Figure 2a), with a ~2-fold increase in active, assembled RuBisCO protein measured under 2% CO_2 (Figure 2d,e). Thus, we established that Syn02 is a suitable model to evaluate the impact of RuBisCO overexpression on downstream physiology and isotopic discrimination. We also observed that higher levels of CO_2 result in increased RuBisCO transcription for both WT and Syn02 strains relative to ambient air. This result is consistent with previous studies reporting the sensitivity of RuBisCO expression to CO_2 (Gesch et al., 2003; Onizuka et al., 2002; Sengupta et al., 2019).

Our experimental approach also enabled us to detect potential upper bounds on the ability of *S. elongatus* to overexpress RuBisCO under a variety of CO_2 conditions. First, increased *rbcL* transcription in Syn02 relative to WT did not always result in a proportional increase in translated RuBisCO protein. For example, even though Syn02 showed a ~14-fold increase in *rbcL* transcript relative to WT in air (Figure 2a), total Syn02 RbcL protein only increased by ~3-fold under these same conditions (Figure 2c). These results indicate that other physiological factors, possibly including RuBisCO translation rate/accuracy or expression of ancillary proteins in our experimental system, may ultimately limit RuBisCO expression

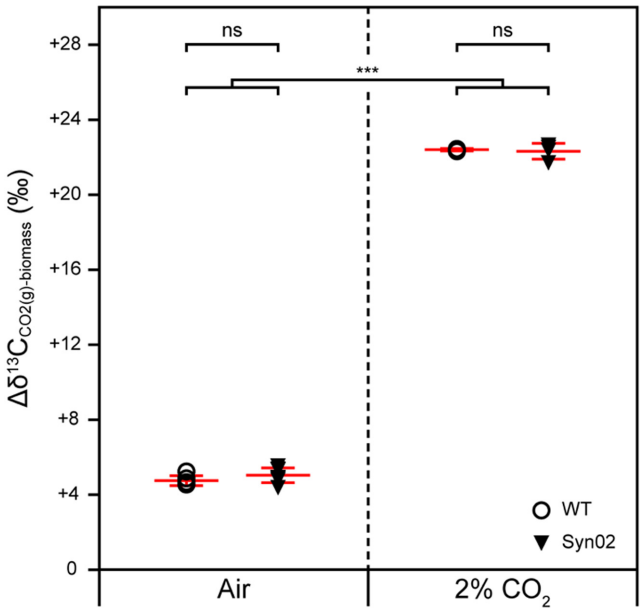

FIGURE 4 $^{13}C/^{12}C$ discrimination associated with photosynthetic CO_2 fixation (ε_p) of *S. elongatus* strains under ambient and 2% CO_2 concentrations. $\Delta\delta^{13}C_{CO2(g)\text{-}biomass}$ values are calculated relative to measured $\delta^{13}C_{CO2}$ (Table S3; see Materials and Methods for calculation). Mean (long horizontal bars) and ±1 SD (vertical error bars) are shown in red, calculated for seven (air) and four (2% CO_2) biological replicates. Asterisks indicate *t*-test results for pairwise comparisons indicated by horizontal lines. Ns, Not significant; ***$p < .001$.

beyond transcription. Further, it is important to consider whether all translated RuBisCO protein is catalytically active. Previous studies have shown that overexpression of RuBisCO in cyanobacteria generally produces an increased pool of active carboxylase (Atsumi et al., 2009; Iwaki et al., 2006; Lechno-Yossef et al., 2020; Liang & Lindblad, 2017). Indeed, for cells grown in 2% CO_2, we found that nearly all overexpressed RuBisCO protein was likely to be assembled and catalytically active (Figure 2c,e). Future work may determine whether this proportion of active, overexpressed RuBisCO holds for cells cultivated at other CO_2 conditions. Finally, we observed that the impact of a second *rbc* copy in Syn02 on *rbcL* transcription was dampened at elevated CO_2 relative to air (Figure 2a), suggesting a potential limit to the combined expression-level effects of increased *rbc* copy number and increased CO_2. Altogether, our findings suggest the presence of physiological constraints that may be limiting RuBisCO overexpression at both transcript and protein levels, the exact mechanism of which awaits further characterization. Similar approaches investigating other model microbial systems would clarify the degree to which these observations might extend to cyanobacteria gene regulation in the past.

We investigated whether the overexpression of RuBisCO in strain Syn02 impacted the growth characteristics of *S. elongatus* and, by that manner, might have the potential to influence isotopic discrimination (Bidigare et al., 1997; Laws et al., 1997; Wilkes et al., 2018). Although various culture conditions including pH, temperature, CO_2 concentration, nutrient availability, and light intensity may substantially affect the growth characteristics of cyanobacteria (Kuan et al., 2015; Rillema et al., 2020; Ungerer et al., 2018; Yu et al., 2015), the influence of genetic factors, including the regulation of RuBisCO expression, is less well known. Previous studies targeting the correlation between RuBisCO overexpression and cyanobacterial physiology have yielded mixed results. For instance, faster growth rates and oxygen evolution rates were observed for an engineered *Synechocystis* PCC 6803 strain that overexpresses RuBisCO (Liang & Lindblad, 2017), as well as in *S. elongatus* upon co-overexpression of its phosphoribulokinase (Kanno et al., 2017). However, in *Synechococcus* sp. PCC 7002, the overexpression of RuBisCO did not alter growth rate (De Porcellinis et al., 2018). The impact of RuBisCO upregulation on cyanobacterial growth appears to be species/strain-specific. Our data show that RuBisCO overexpression in *S. elongatus* PCC 7942 strain Syn02 results in a minor increase in growth rate in ambient air relative to WT, and no significant difference in growth or oxygen evolution rates was observed at elevated CO_2 levels. Our results indicate that further study is needed to fully understand the coupled interaction of different environmental conditions and genetic backgrounds in determining cyanobacterial growth parameters of relevance to carbon biosignature generation.

We found that the degree of RuBisCO overexpression generated in Syn02 did not measurably impact *S. elongatus* $\delta^{13}C_{biomass}$, neither did it affect isotopic fractionation between biomass and the source carbon ($\delta^{13}CO_{2(g)}$) (Figure 4). Rather, inorganic carbon availability had the overriding influence, an effect that has previously been observed empirically for a variety of autotrophs (Freeman & Hayes, 1992; Hinga et al., 1994; Schubert & Jahren, 2012; Wilkes et al., 2018), including for cyanobacteria in particular (Eichner et al., 2015; Hurley et al., 2021). The calculation of ε_p under ambient CO_2 was not possible in our experimental setup as the system was not at equilibrium. The small fractionation difference found between the source carbon and biomass along with slower growth rates under ambient air suggests the system was considerably carbon limited. Under carbon limitation and a nonequilibrium system, a number of factors can influence $\delta^{13}C_{biomass}$, including Rayleigh fractionation, kinetic isotope effects on the conversion of inorganic carbon species (which are often significantly different to the equilibrium isotope effects (Yumol et al., 2020)), and CCM activity (Hurley et al., 2021). Though we are unable to calculate ε_p under ambient air, it should be noted that high pH, dense biomass, and carbon limitation are representative of phytoplankton blooms and cyanobacterial mats (Borovec et al., 2010; Jensen et al., 2011; Wilhelm et al., 2020). The geological record often requires the assumption of equilibrium when using $\delta^{13}C$ of carbonates and total organic carbon ($\delta^{13}C_{carb}$, $\delta^{13}C_{TOC}$) to draw inferences about atmospheric composition. However, we consider that in some cases where the majority of biological deposition routinely occurs during periods of high biomass (i.e., cyanobacterial mats or blooms), nonequilibrium systems may dominate and influence paleoreconstructions.

Under 2% CO_2 (a concentration within the estimated range of Precambrian atmospheric CO_2 (Catling & Zahnle, 2020)), we observed a larger fractionation between $CO_{2(g)}$ and cyanobacterial biomass. Theoretically, under high CO_2 concentrations, RuBisCO is able to exert close to its full intrinsic kinetic isotope effect (KIE), maximizing ε_p (Bidigare et al., 1997; Hayes, 1993; Schubert & Jahren, 2012; Wilkes et al., 2018). Under 2% CO_2 this system was close to equilibrium. We thus approximated ε_p from calculated $\delta^{13}C_{CO2(aq)}$, which was found to be ~23‰, close to the measured KIE for cyanobacterial Form IA and IB RuBisCO at saturating CO_2 of ~22‰–24‰ (Guy et al., 1993; Scott et al., 2007). Nevertheless, these results should be treated with caution as we did not measure RuBisCO KIE in vitro, and other factors such as other biological processes (including carbon-concentrating mechansims, organic composition) and quasi-equilibrium could impact the whole-cell, isotopic signatures observed in our experimental system (Burnap et al., 2015; Eichner et al., 2015; Hurley et al., 2021; Wilkes & Pearson, 2019).

It is apparent that the increased RuBisCO expression and total protein carboxylase activity in Syn02 exerts little impact on $^{13}C/^{12}C$ of cyanobacterial biomass. ε_p of ancient cyanobacteria falls within the ~8‰–24‰ range inferred from the Precambrian carbon isotope record following the rise of atmospheric oxygen (Hurley et al., 2021; Krissansen-Totton et al., 2015). Our data suggest that potential overexpression of RuBisCO by past cyanobacterial primary producers likely does not help explain the distribution of Precambrian carbon biosignatures. Rather, it is more probable that other environmental and intracellular factors, including but not limited to CO_2 levels, growth rates, temperature, and CCM effects, as well as taxonomic and RuBisCO form variability (reviewed by Garcia et al. (2021)), are more significant determinants of the isotopic compositions of organic carbon. Nevertheless, our results provide an important control for future investigations of carbon fixation signatures based on engineered, model microbial systems. Such studies would likely generate RuBisCO expression variability as a function of environmental or genetic manipulations, as was observed in the isotopic characterization of a cyanobacterium hosting an inferred, Precambrian RuBisCO (Kedzior et al., 2022). Explicit investigations of regulatory dynamics associated with ancient carbon fixation, by strategies including the phylogenetic reconstruction of ancestral regulatory pathways and promoter sequences, would reveal whether the carbon fixation signatures of ancient primary producers might be impacted beyond the RuBisCO expression variability tested here. Further integrative laboratory approaches addressing these factors are crucial to expand the utility of modern organismal proxies in interpreting evidence for microbial activity on Earth.

4 | MATERIALS AND METHODS

4.1 | Cyanobacterial growth and maintenance

Synechococcus elongatus PCC 7942 strains were cultured in BG-11 medium (Rippka et al., 1979) as liquid cultures or on agar plates (1.5% (w/v) agar and 1 mM $Na_2S_2O_3{\cdot}5H_2O$). For recombinant strains, liquid and solid media were supplemented with appropriate antibiotics: 2 μg·ml^{-1} Spectinomycin (Sp) plus 2 μg ml^{-1} Streptomycin (Sm), 5 μg ml^{-1} Kanamycin (Km). The cyanobacterial growth was measured by optical density at 750 nm (OD_{750}).

The strains were archived at −80°C in 15% (v/v) glycerol. The 2-ml glycerol stocks were rapidly thawed and inoculated in liquid BG-11 (supplemented with antibiotics as needed). Liquid cultures were maintained in a Percival environment chamber (Cat. No. I36LLVLC8) fitted to a CO_2 gas cylinder input, permitting monitoring and control of internal atmospheric CO_2. Cultures were shaken at 120 rpm at 30°C under continuous low illumination of 45 μmol photon·m^{-2} s^{-1}, and ambient air, until they reached an OD_{750} between 0.4 and 0.6. These cultures were then used to inoculate fresh cultures that were grown using similar conditions but under continuous, moderate illumination of 80 μmol photon·m^{-2} s^{-1} (following (Smith & Williams, 2006); growth saturation has been observed at illumination levels greater than 120 μmol photon·m^{-2} s^{-1}) and sparged at selected CO_2 concentrations (ambient air, 2%, or 5% CO_2; cultures were also grown without sparging for carbon isotope fractionation experiments and to assess differences in growth rate; Table S1). Cultures were sampled at an OD_{750} of ~7 to 7.5 for most subsequent experiments, as described below. Cultures were sampled at an earlier OD_{750} of 0.5–1.5 (early exponential growth phase) for carbon isotope fractionation measurement and for additional RT-qPCR experiments (Figure S1).

4.2 | Genetic engineering of cyanobacteria

A recombinant strain of *S. elongatus* was constructed by natural transformation using standard protocols (Clerico et al., 2007) and the plasmids and methods described below (Table 1). To construct the plasmid pSyn02, pAM4937 was digested with *Swa*I to release the *ccdB* toxic gene and produce a plasmid backbone that contains the pBR322 *E. coli* origin of replication, the base of mobilization site for conjugal transfer, the *aph1* gene conferring kanamycin resistance, and sequences for homologous recombination into *S. elongatus* chromosome at NS2. The *rbc* operon was amplified from *S. elongatus* PCC 7942 gDNA with primers F01 and R01 (Table S4) containing 20-nucleotide sequences that overlap with pAM4937 backbone. The resulting DNA fragments were assembled using the GeneArt™ Seamless Cloning and Assembly Kit (Invitrogen, Cat. No. A13288). pSyn02 was used to insert the *rbc* operon into NS2 of the wild-type genome in the strain PCC 7942 through homologous recombination to create the strain of *S. elongatus*, Syn02, carrying two copies of the *rbc* operon. Plasmid pSyn-01 was constructed by using two primer pairs F02/R02 and F03/R03 (Table S4), (1) to amplify a fragment of pAM4951 that contains the *E. coli* origin of replication and the site for conjugal transfer, and (2) to amplify the *aadA* gene conferring spectinomycin/streptomycin resistance. Native *rbc* operon flanking sequences were amplified from the *S. elongatus* PCC 7942 gDNA with the primer pairs F04/R04 and F05/R05 (Table S4) containing 20-nucleotide sequences that overlap with the pAM4951 fragments.

Transformation was carried out after growing the WT strain in liquid culture at 30 °C with shaking (120 rpm) and a light intensity of 80 μmol photon·m^{-2} s^{-1} until an OD_{750} ~ 0.7. The cells were prepared for transformation according to the protocol by Clerico et al. (2007) and plated on BG-11 agar containing the appropriate antibiotic(s) for recovery. Subsequently, the colonies were picked using sterile pipette tips, patched onto BG-11 agar containing the appropriate antibiotic(s), and further incubated to ensure complete chromosome segregation (i.e., incorporation of the *trans*-gene into all chromosomes). The patched transformants were screened using colony PCR using the primers F06/R06 and F07/R07 and the genotypes of the engineered strains were confirmed by Sanger sequencing using the primers F08/R08 (Figure S3, Table S4).

4.3 | Extraction of total RNA and proteins

Cultures were collected during the exponential growth phase. Cells were pelleted by centrifugation at 4700 × g for 10 min at room temperature and resuspended in 10 ml of TE buffer (10 mM Tris, pH 8.0, 1 mM EDTA). To prepare the crude cell lysate, 8 ml of the cell suspension were pelleted by centrifugation at 4700 × g for 10 min at room temperature, resuspended in 500 μl of hot (pre-warmed to 95°C) TE buffer supplemented with 1% (w/v) SDS and incubated at 95°C for 10 min. The mixture was sonicated at 40% amplitude for 3 × 10 s with 10 s intervals and the cell debris was centrifuged at 17,000 × g for 10 min at room temperature. The supernatant was collected and stored at −80°C. Total RNA was extracted from the remaining 2 ml of the cell suspension using the RNeasy® Protect Bacteria Mini Kit (QIAGEN, Cat. No. 74524) following the manufacturer instructions.

4.4 | Analysis of *rbc* operon expression by RT-qPCR

Total RNA was quantified with a NanoDrop spectrophotometer and 1 μg of RNA was treated with the amplification grade deoxyribonuclease I (Invitrogen, Cat. No. 18068-015). Ten microliters of DNase I-treated RNA was then used for reverse transcription (RT) performed with the SuperScript™ IV First-Strand Synthesis System (Invitrogen, Cat. No. 18091050). The four pairs of qPCR primers (listed in Table S4) were designed with Primer3Plus (http://www.bioinformatics.nl/cgi-bin/primer3plus/primer3plus.cgi). Both reference genes have previously been shown to be stably expressed under diverse conditions in *S. elongatus* (Luo et al., 2019). The quality of cDNA and primer specificity was assessed by PCR using cDNA templates (RT positive reactions), RT negative controls, and the qPCR primers. The analysis of gene expression levels was performed in a real-time thermal cycler qTOWER^3 G (Analytik Jena AG), equipped with the qPCRsoft software, using the cycles: 50°C/2 min, 95°C/2 min, 40 × (95°C/15 s, 60°C/1 min). The relative expression of the *rbc* operon genes (*rbcL* and *purK*) was calculated as the average fold change normalized to *secA or ppc* reference genes using the delta–delta Ct method. The experiment was carried out using three biological replicates and three technical replicates.

4.5 | Analysis of RbcL protein by Western blot

Total protein concentration in the crude cell lysates was measured using the Pierce™ BCA Protein Assay Kit (Thermo Scientific, Cat. No. 23225). The lysates were loaded in the amount of 5 μg of total protein in Laemmli sample buffer onto a 6% (v/v) polyacrylamide stacking gel. Proteins were electrophoresed in a 12% polyacrylamide resolving gel in TGS buffer and blotted in transfer buffer onto a PVDF membrane. Total protein load in each sample was visualized by Revert™ 700 Total Protein Stain (LI-COR Biosciences, Cat. No. 926-11011) and used for RbcL signal normalization. Detection of RbcL was performed by overnight incubation of the membrane at 4°C with rabbit anti-RbcL antibody (Agrisera, Cat. No. AS03 037), 1:5000 in TBST with 5% nonfat milk, followed by 1-h incubation at room temperature with IRDye® 800CW goat antirabbit IgG secondary antibody (LI-COR Biosciences, Cat. No. 926-32211), 1:20,000 in Intercept® (TBS) blocking buffer (LI-COR Biosciences, Cat. No. 927-60001) with 0.1% (v/v) Tween-20 and 0.01% (w/v) SDS. Both the total protein load and the amount of RbcL in each sample were documented with Odyssey® Fc Imaging System (LI-COR Biosciences, Cat. No. 2800-03) at the near-infrared detection mode. The images were acquired using Image Studio™ software. The densitometric analysis of RbcL signal intensity, normalized to total protein load, was performed with Quantity One® software (Bio-Rad) for six biological replicates. The amount of RbcL produced by each replicate of the Syn02 strain culture was compared to the averaged level of RbcL in the WT PCC 7942 replicate cultures and expressed as the averaged percent of RbcL synthesized by the WT strain.

4.6 | Assembly of RuBisCO subunits

Assembly of the RuBisCO large and small subunits into a hexadecameric complex in each strain was evaluated by native gel electrophoresis and immunodetection. Samples were collected during the exponential growh phase. Cells grown under 2% CO_2 were pelleted by centrifugation at 4700 × *g* for 10 min at room temperature and resuspended in 400 μl of native lysis buffer (50 mM Tris, pH 8.0, 150 mM NaCl, 1 mM EDTA, 10% (v/v) glycerol) supplemented with 5 mM DTT, 100 μg/ml lysozyme from chicken egg white, and 1% (v/v) Halt™ Protease Inhibitor Cocktail (Thermo Scientific, Cat. No. 78430). The cell suspensions were incubated at 30°C for 15 min and subjected to five consecutive freeze–thaw cycles (10 min at −80°C followed by 5 min at 30°C), then were sonicated on ice for 3 min at 30% amplitude (2-s on/off intervals), centrifuged at 17,000 × *g* for 15 min at 4°C. The concentration of total soluble proteins in the lysates was determined with a Pierce™ BCA Protein Assay Kit. The lysates were adjusted to 5 μg of total

soluble proteins in native sample buffer and then loaded onto a 4%–20% Mini-PROTEAN® TGX™ Precast Protein Gel (Bio-Rad, Cat. No. 4561094). Protein electrophoreses were performed in TG buffer (60 mM Tris, 192 mM glycine) at 100 V for 4 h at 4°C and blotted in transfer buffer (48 mM Tris, pH 9.2, 39 mM glycine, 0.04% (w/v) SDS) onto a nitrocellulose membrane. After three 10-min washes in wash buffer (48 mM Tris, pH 9.2, 39 mM glycine, 20% (v/v) methanol), total protein load in each sample was visualized by Revert™ 700 Total Protein Stain and used for the normalization of RuBisCO complex quantity. Immunodetection of the RuBisCO complex was performed with the same primary and secondary antibodies that were used to analyze the level of RbcL, as described above.

4.7 | Catalytic activity of RuBisCO

The activity of RuBisCO in cyanobacterial lysates was measured using a spectrophotometric coupled-enzyme assay that links this activity with the rate of NADH oxidation (Kubien et al., 2011). The cyanobacterial strains were cultured under 2% CO_2, collected, and pelleted as described above. The pellets were resuspended in 1 ml of ice-cold lysis buffer (50 mM EPPS, 1 mM EDTA, 2 mM DTT, pH 8.0) and transferred into 2 ml screw-capped tubes with Lysing Matrix B (MP Biomedical) for lysis by bead beating using FastPrep-24™ 5G bead beater (MP Biomedical) with 4 m/s for 10 s, followed by 2-min incubation on ice, repeated six times. The cell lysates were transferred to new Eppendorf tubes to remove the beads and unbroken cells and to pellet the thylakoid membrane by centrifugation at 10,000 × g for 1 min and at 20,000 × *g* for 30 min at 4°C, sequentially. The resulting clear supernatants containing cytosolic soluble proteins, including phycobiliproteins and RuBisCO, were used to determine protein concentration by Pierce™ BCA Protein Assay Kit and to measure RuBisCO activity by employing an assay adapted from Kubien et al. (2011). The assay buffer (100 mM HEPES, 25 mM $MgCl_2$, 1 mM EDTA, pH 7.6) was used considering the high Michaelis constant for CO_2 (K_C) for cyanobacterial RuBisCO. 20 μl of cell lysates were preincubated in the assay mix (with 5 mM $NaHCO_3$) at 25 °C for activation before initiating the reaction by adding synthesized ribulose 1,5-bisphosphate (RuBP) according to Kane et al. (1998). The absorbance at 340 nm was monitored using a Synergy H1 plate reader (BioTek). RuBisCO activity was reported as RuBP consumption rate normalized to total soluble protein content. The assay was performed for three biological replicates.

4.8 | Cyanobacterial growth measurements

OD_{750} values were plotted as a function of time and analyzed in R with the Growthcurver package. Growth curve data was fitted to the standard form of the logistic equation to calculate growth parameters including growth rate, doubling time, and carrying capacity (Sprouffske & Wagner, 2016). Each strain was grown in triplicate for every condition.

4.9 | Photosynthetic oxygen evolution rate

Synechococcus elongatus strain photosynthetic activity was assayed using a Clark-type oxygen electrode chamber to measure the level of molecular oxygen produced in cyanobacterial cultures. Cells were grown in 50 ml of BG-11 at 30°C, illumination of 80 μmol photon·m^{-2}·s^{-1}, shaking at 120 rpm, in ambient air, and with culture sparging. The samples were collected from triplicate cultures during the exponential growth phase, pelleted by centrifugation at 4700 × g for 10 min at room temperature, and resuspended in fresh BG-11 to an OD_{750} of ~1.0. Oxygen evolution rates were normalized to chlorophyll *a* concentration following (Liang & Lindblad, 2017) using the protocol by Zavřel et al. (2015). The remaining suspension was incubated in the dark for 20 min with gentle agitation. Samples from each suspension, prepared in three technical replicates, were analyzed in an oxygen electrode chamber under saturated light, using the Oxygraph+ System (Hansatech Instruments) equipped with the OxyTrace+ software. Oxygen evolution rate was monitored for 10 min and expressed as nanomoles of molecular oxygen evolved per hour per microgram of chlorophyll *a*.

4.10 | Carbon isotope fractionation in bulk cyanobacterial biomass

Carbon isotope fractionation experiments were conducted under ambient and 2% CO_2 conditions. Cyanobacteria were cultured in shaken flasks (all other conditions as described above) to an OD_{750} of 0.5–1.5 in the early exponential growth phase (seven and four biological replicates per strain for experiments conducted in air and 2% CO_2, respectively). Cells were pelleted by centrifugation at 4700 × *g* for 10 min at room temperature and washed in 10 ml of 10 mM NaCl. The bacteria were resuspended in 1 ml of 10 mM NaCl and transferred to Eppendorf tubes. After centrifugation at 4700 × *g* for 10 min at room temperature, the supernatant was completely removed, the pellets were dried in opened tubes in a laboratory oven at 50°C for 2 days, and the resultant dried biomass samples were transferred into tin capsules. Growth medium aliquots were sampled both prior to culture inoculation and alongisde cell harvest during the early exponential phase (see above) for pH measurement. Aliquots sampled alongside cell harvest were filter-sterilized (0.2 μm), transferred to Extetainer vials leaving no headspace, and stored at 4°C for DIC concentration and $\delta^{13}C_{DIC}$ measurement. Finally, internal incubator gas was sampled for ambient and 2% CO_2 experiments, as well as CO_2 gas cylinders used to mix 2% CO_2, following the sample collection protocol provided by the UC Davis Stable Isotope Facility.

The carbon isotope composition of bulk biomass ($\delta^{13}C_{biomass}$), DIC ($\delta^{13}C_{DIC}$), and CO_2 ($\delta^{13}C_{CO2(g)}$) samples was determined at the UC Davis Stable Isotope Facility. $\delta^{13}C_{biomass}$ was analyzed using

a PDZ Europa ANCA-GSL elemental analyzer interfaced to a PDZ Europa 20–20 isotope ratio mass spectrometer (Sercon Ltd.). $\delta^{13}C_{DIC}$ (prepared by CO_2 gas evolution using 85% phosphoric acid) and $\delta^{13}C_{CO2(g)}$ were measured by a GasBench II system interfaced to a Delta V Plus IRMS (Thermo Scientific). All carbon isotopic composition values are reported relative to the Vienna PeeDee Belemnite standard (V-PDB):

$$\delta\,^{13}C_{sample}[‰] = \left(\frac{^{13}C/\,^{12}C_{sample}}{^{13}C/\,^{12}C_{V-PDB}} - 1\right) \times 1000$$

For cultures grown at 2% CO_2, the carbon isotope fractionation associated with photosynthetic CO_2 fixation (ε_p) was calculated from $\delta^{13}C_{biomass}$ and $\delta^{13}C_{CO2(aq)}$ according to Freeman and Hayes (1992):

$$\varepsilon_p[‰] = \left(\frac{\delta\,^{13}C_{CO2(aq)} + 1000}{\delta\,^{13}C_{biomass} + 1000} - 1\right) \times 1000$$

$\delta^{13}C_{CO2(aq)}$ was calculated from measured $\delta^{13}C_{DIC}$ following the equation provided by Rau et al. (1996), based on Mook et al. (1974):

$$\delta\,^{13}C_{CO2(aq)}[‰] = \delta\,^{13}C_{DIC} + 23.644 - \frac{9701.5}{T_K}$$

where T_K is the absolute temperature in Kelvin.

The calculation of ε_p requires a system in equilibrium to estimate $CO_{2(aq)}$, though we note that some studies describe ε_p as the difference between $\delta^{13}C_{CO2(g)}$ and $\delta^{13}C_{biomass}$ (Heureux & Rickaby, 2015). Thus, for cultures grown under ambient CO_2 (non-equilibrium conditions), we calculated the isotopic deviation between the inorganic carbon source ($\delta^{13}C_{CO2(g)}$) and the dissolved inorganic carbon pool ($\delta^{13}C_{DIC}$):

$$\Delta\delta\,^{13}C_{CO2(g)-DIC}[‰] = \delta\,^{13}C_{CO2(g)} - \delta\,^{13}C_{DIC}$$

as well as between $\delta^{13}C_{CO2(g)}$ and $\delta^{13}C_{biomass}$:

$$\Delta\delta\,^{13}C_{CO2(g)-biomass}[‰] = \delta\,^{13}C_{CO2(g)} - \delta\,^{13}C_{biomass}$$

4.11 | Statistical analyses

Results for experimental analyses were presented as the mean and the sample standard deviation (SD) values of at least three independent experiments. Statistical significance was analyzed with the two-tailed *t*-test. The unpaired sample *t*-test assuming equal variances was used to compare the values obtained for different cyanobacterial strains and the paired sample *t*-test was used to compare the values for the same strain at different experimental conditions.

FUNDING INFORMATION

This work was supported by the National Science Foundation Emerging Frontiers Program Award No. 1724090 (BK), NASA Early Career Faculty (ECF) Award No. 80NSSC19K1617 (BK), NASA Postdoctoral Fellowship (AKG), Simons Foundation Early Career Award No. 561645 (JNY and ML), and National Institute of General Medical Sciences of the National Institutes of Health award number R01GM118815 (AT, to James W. Golden at the University of California-San Diego).

DATA AVAILABILITY STATEMENT

The data that support the findings of this study are available from the corresponding author upon reasonable request.

ORCID

Amanda K. Garcia https://orcid.org/0000-0002-1936-2568
Arnaud Taton https://orcid.org/0000-0001-5494-5964
Meng Li https://orcid.org/0000-0001-9831-8575
Jodi N. Young https://orcid.org/0000-0002-3156-8403
Betül Kaçar https://orcid.org/0000-0002-0482-2357

REFERENCES

Andersson, C. R., Tsinoremas, N. F., Shelton, J., Lebedeva, N. V., Yarrow, J., Min, H., & Golden, S. S. (2000). Application of bioluminescence to the study of circadian rhythms in cyanobacteria. *Methods in Enzymology*, *305*, 527–542.

Atsumi, S., Higashide, W., & Liao, J. C. (2009). Direct photosynthetic recycling of carbon dioxide to isobutyraldehyde. *Nature Biotechnology*, *27*(12), 1177–1180. https://doi.org/10.1038/nbt.1586

Bar-On, Y. M., & Milo, R. (2019). The global mass and average rate of rubisco. *Proceedings of the National Academy of Sciences of the United States of America*, *10*, 4738–4743. https://doi.org/10.1073/pnas.1816654116

Bidigare, R. R., Fluegge, A., Freeman, K. H., Hanson, K. L., Hayes, J. M., Hollander, D., Jasper, J. P., King, L. L., Laws, E. A., Milder, J., Millero, F. J., Pancost, R., Popp, B. N., Steinberg, P. A., & Wakeham, S. G. (1997). Consistent fractionation of ^{13}C in nature and in the laboratory: Growth-rate effects in some haptophyte algae. *Global Biogeochem Cycles*, *11*(2), 279–292. https://doi.org/10.1029/96gb03939

Boller, A. J., Thomas, P. J., Cavanaugh, C. M., & Scott, K. M. (2011). Low stable carbon isotope fractionation by coccolithophore RubisCO. *Geochimica et Cosmochimica Acta*, *75*(22), 7200–7207. https://doi.org/10.1016/j.gca.2011.08.031

Boller, A. J., Thomas, P. J., Cavanaugh, C. M., & Scott, K. M. (2015). Isotopic discrimination and kinetic parameters of RubisCO from the marine bloom-forming diatom, *Skeletonema costatum*. *Geobiology*, *13*(1), 33–43. https://doi.org/10.1111/gbi.12112

Bonfil, D. J., Ronen-Tarazi, M., Sultemeyer, D., Lieman-Hurwitz, J., Schatz, D., & Kaplan, A. (1998). A putative HCO_3^- transporter in the cyanobacterium Synechococcus sp. strain PCC 7942. *FEBS Letters*, *430*(3), 236–240.

Borovec, J., Sirová, D., Mošnerová, P., Rejmánková, E., & Vrba, J. (2010). Spatial and temporal changes in phosphorus partitioning within a freshwater cyanobacterial mat community. *Biogeochemistry*, *101*(1–3), 323–333. https://doi.org/10.1007/s10533-010-9488-4

Burnap, R., Hagemann, M., & Kaplan, A. (2015). Regulation of CO_2 concentrating mechanism in cyanobacteria. *Life*, *5*(1), 348–371. https://doi.org/10.3390/life5010348

Carroll, S. B. (2005). Evolution at two levels: On genes and form. *PLoS Biology*, *3*(7), e245. https://doi.org/10.1371/journal.pbio.0030245

Catling, D. C., & Zahnle, K. J. (2020). The Archean atmosphere. *Science Advances*, *6*(9), eaax1420. https://doi.org/10.1126/sciadv.aax1420

Cernusak, L. A., Ubierna, N., Winter, K., Holtum, J. A., Marshall, J. D., & Farquhar, G. D. (2013). Environmental and physiological

determinants of carbon isotope discrimination in terrestrial plants. *New Phytologist*, *200*(4), 950–965. https://doi.org/10.1111/nph.12423

Clerico, E. M., Ditty, J. L., & Golden, S. S. (2007). Specialized techniques for site-directed mutagenesis in cyanobacteria. *Methods in Molecular Biology*, *362*, 155–171. https://doi.org/10.1007/978-1-59745-257-1_11

De Porcellinis, A. J., Norgaard, H., Brey, L. M. F., Erstad, S. M., Jones, P. R., Heazlewood, J. L., & Sakuragi, Y. (2018). Overexpression of bifunctional fructose-1,6-bisphosphatase/sedoheptulose-1,7-bisphosphatase leads to enhanced photosynthesis and global reprogramming of carbon metabolism in Synechococcus sp. PCC 7002. *Metabolic Engineering*, *47*, 170–183. https://doi.org/10.1016/j.ymben.2018.03.001

Deleens, E., Treichel, I., & O'Leary, M. H. (1985). Temperature dependence of carbon isotope fractionation in CAM plants. *Plant Physiology*, *79*(1), 202–206. https://doi.org/10.1104/pp.79.1.202

Des Marais, D. J. (2001). Isotopic evolution of the biogeochemical carbon cycle during the Precambrian. *Reviews in Mineralogy and Geochemistry*, *43*(1), 555–578. https://doi.org/10.2138/gsrmg.43.1.555

Eek, M. K., Whiticar, M. J., Bishop, J. K. B., & Wong, C. S. (1999). Influence of nutrients on carbon isotope fractionation by natural populations of Prymnesiophyte algae in NE Pacific. *Deep Sea Research Part II: Topical Studies in Oceanography*, *46*(11–12), 2863–2876. https://doi.org/10.1016/s0967-0645(99)00086-7

Eichner, M., Thoms, S., Kranz, S. A., & Rost, B. (2015). Cellular inorganic carbon fluxes in *Trichodesmium*: A combined approach using measurements and modelling. *Journal of Experimental Botany*, *66*(3), 749–759. https://doi.org/10.1093/jxb/eru427

Ellis, R. J. (1979). The most abundant protein in the world. *Trends in Biochemical Sciences*, *4*(11), 241–244.

Erb, T. J., & Zarzycki, J. (2018). A short history of RubisCO: The rise and fall (?) of Nature's predominant CO_2 fixing enzyme. *Current Opinion in Biotechnology*, *49*, 100–107. https://doi.org/10.1016/j.copbio.2017.07.017

Falkowski, P. G., Fenchel, T., & Delong, E. F. (2008). The microbial engines that drive Earth's biogeochemical cycles. *Science*, *320*(5879), 1034–1039. https://doi.org/10.1126/science.1153213

Fay, J. C., & Wittkopp, P. J. (2008). Evaluating the role of natural selection in the evolution of gene regulation. *Heredity (Edinb)*, *100*(2), 191–199. https://doi.org/10.1038/sj.hdy.6801000

Field, C. B. (1998). Primary production of the biosphere: Integrating terrestrial and oceanic components. *Science*, *281*(5374), 237–240. https://doi.org/10.1126/science.281.5374.237

Freeman, K. H., & Hayes, J. M. (1992). Fractionation of carbon isotopes by phytoplankton and estimates of ancient CO_2 levels. *Global Biogeochemical Cycles*, *6*(2), 185–198. https://doi.org/10.1029/92gb00190

Gabay, C., Lieman-Hurwitz, J., Hassidim, M., Ronen-Tarazi, M., & Kaplan, A. (1998). Modification of topA in Synechococcus sp. PCC 7942 resulted in mutants capable of growing under low but not high concentration of CO2. *FEMS Microbiology Letters*, *159*(2), 343–347. https://doi.org/10.1111/j.1574-6968.1998.tb12881.x

Garcia, A. K., Cavanaugh, C. M., & Kacar, B. (2021). The curious consistency of carbon biosignatures over billions of years of earth-life coevolution. *The ISME Journal*, *15*, 2183–2194. https://doi.org/10.1038/s41396-021-00971-5

Gesch, R. W., Kang, I. H., Gallo-Meagher, M., Vu, J. C. V., Boote, K. J., Allen, L. H., & Bowes, G. (2003). Rubisco expression in rice leaves is related to genotypic variation of photosynthesis under elevated growth CO_2 and temperature. *Plant, Cell & Environment*, *26*(12), 1941–1950. https://doi.org/10.1046/j.1365-3040.2003.01110.x

Guy, R. D., Fogel, M. L., & Berry, J. A. (1993). Photosynthetic fractionation of the stable isotopes of oxygen and carbon. *Plant Physiology*, *101*(1), 37–47. https://doi.org/10.1104/pp.101.1.37

Hamilton, T. L., Bryant, D. A., & Macalady, J. L. (2016). The role of biology in planetary evolution: Cyanobacterial primary production in low-oxygen Proterozoic oceans. *Environmental Microbiology*, *18*(2), 325–340. https://doi.org/10.1111/1462-2920.13118

Havig, J. R., Hamilton, T. L., Bachan, A., & Kump, L. R. (2017). Sulfur and carbon isotopic evidence for metabolic pathway evolution and a four-stepped earth system progression across the Archean and Paleoproterozoic. *Earth-Science Reviews*, *174*, 1–21. https://doi.org/10.1016/j.earscirev.2017.06.014

Hayes, J. M. (1993). Factors controlling ^{13}C contents of sedimentary organic compounds: Principles and evidence. *Marine Geology*, *113*(1–2), 111–125. https://doi.org/10.1016/0025-3227(93)90153-m

Hayes, J. M. (2001). Fractionation of carbon and hydrogen isotopes in biosynthetic processes. *Reviews in Mineralogy and Geochemistry*, *43*(1), 225–277. https://doi.org/10.2138/gsrmg.43.1.225

Heureux, A. M. C., & Rickaby, R. E. M. (2015). Refining our estimate of atmospheric CO_2 across the Eocene–Oligocene climatic transition. *Earth and Planetary Science Letters*, *409*, 329–338. https://doi.org/10.1016/j.epsl.2014.10.036

Hill, W. R., Fanta, S. E., & Roberts, B. J. (2008). 13C dynamics in benthic algae: Effects of light, phosphorus, and biomass development. *Limnology and Oceanography*, *53*(4), 1217–1226. https://doi.org/10.4319/lo.2008.53.4.1217

Hinga, K. R., Arthur, M. A., Pilson, M. E. Q., & Whitaker, D. (1994). Carbon isotope fractionation by marine phytoplankton in culture: The effects of CO_2 concentration, pH, temperature, and species. *Global Biogeochemical Cycles*, *8*(1), 91–102. https://doi.org/10.1029/93gb03393

Hood, R. D., Higgins, S. A., Flamholz, A., Nichols, R. J., & Savage, D. F. (2016). The stringent response regulates adaptation to darkness in the cyanobacterium Synechococcus elongatus. *Proceedings of the National Academy of Sciences of the United States of America*, *113*(33), E4867–E4876. https://doi.org/10.1073/pnas.1524915113

Hurley, S. J., Wing, B. A., Jasper, C. E., Hill, N. C., & Cameron, J. C. (2021). Carbon isotope evidence for the global physiology of Proterozoic cyanobacteria. *Science Advances*, *7*(2), eabc8998. https://doi.org/10.1126/sciadv.abc8998

Iwaki, T., Haranoh, K., Inoue, N., Kojima, K., Satoh, R., Nishino, T., Wada, S., Ihara, H., Tsuyama, S., Kobayashi, H., & Wadano, A. (2006). Expression of foreign type I ribulose-1,5-bisphosphate carboxylase/oxygenase (EC 4.1.1.39) stimulates photosynthesis in cyanobacterium Synechococcus PCC7942 cells. *Photosynthesis Research*, *88*(3), 287–297. https://doi.org/10.1007/s11120-006-9048-x

Jensen, S. I., Steunou, A. S., Bhaya, D., Kuhl, M., & Grossman, A. R. (2011). In situ dynamics of O2, pH and cyanobacterial transcripts associated with CCM, photosynthesis and detoxification of ROS. *The ISME Journal*, *5*(2), 317–328. https://doi.org/10.1038/ismej.2010.131

Kacar, B., Hanson-Smith, V., Adam, Z. R., & Boekelheide, N. (2017). Constraining the timing of the great oxidation event within the rubisco phylogenetic tree. *Geobiology*, *15*(5), 628–640. https://doi.org/10.1111/gbi.12243

Kane, H. J., Wilkin, J.-M., Portis, A. R., & John Andrews, T. (1998). Potent inhibition of ribulose-bisphosphate carboxylase by an oxidized impurity in Ribulose-1,5-bisphosphate. *Plant Physiology*, *117*(3), 1059–1069. https://doi.org/10.1104/pp.117.3.1059

Kanno, M., Carroll, A. L., & Atsumi, S. (2017). Global metabolic rewiring for improved CO2 fixation and chemical production in cyanobacteria. *Nature Communications*, *8*(1), 14724. https://doi.org/10.1038/ncomms14724

Kedzior, M., Garcia, A. K., Li, M., Taton, A., Adam, Z. R., Young, J. N., & Kacar, B. (2022). Resurrected rubisco suggests uniform carbon isotope signatures over geologic time. *Cell Reports*, *39*(4), 110726. https://doi.org/10.1016/j.celrep.2022.110726

Knoll, A. H., & Nowak, M. A. (2017). The timetable of evolution. *Science Advances*, *3*(5), e1603076. https://doi.org/10.1126/sciadv.1603076

Krissansen-Totton, J., Buick, R., & Catling, D. C. (2015). A statistical analysis of the carbon isotope record from the Archean to phanerozoic and implications for the rise of oxygen. *American Journal of Science*, *315*(4), 275–316. https://doi.org/10.2475/04.2015.01

Kuan, D., Duff, S., Posarac, D., & Bi, X. (2015). Growth optimization of Synechococcus elongatus PCC7942 in lab flasks and a 2-D photobioreactor. *The Canadian Journal of Chemical Engineering*, *93*(4), 640–647. https://doi.org/10.1002/cjce.22154

Kubien, D. S., Brown, C. M., & Kane, H. J. (2011). Quantifying the amount and activity of rubisco in leaves. *Methods in Molecular Biology*, *684*, 349–362. https://doi.org/10.1007/978-1-60761-925-3_27

Laws, E. A., Bidigare, R. R., & Popp, B. N. (1997). Effect of growth rate and CO_2 concentration on carbon isotopic fractionation by the marine diatom *Phaeodactylum tricornutum*. *Limnology and Oceanography*, *42*(7), 1552–1560. https://doi.org/10.4319/lo.1997.42.7.1552

Laws, E. A., Popp, B. N., Bidigare, R. R., Kennicutt, M. C., & Macko, S. A. (1995). Dependence of phytoplankton carbon isotopic composition on growth rate and $[CO_2]_{aq}$: Theoretical considerations and experimental results. *Geochimica et Cosmochimica Acta*, *59*(6), 1131–1138. https://doi.org/10.1016/0016-7037(95)00030-4

Laws, E. A., Popp, B. N., Cassar, N., & Tanimoto, J. (2002). ^{13}C discrimination patterns in oceanic phytoplankton: Likely influence of CO_2 concentrating mechanisms, and implications for palaeoreconstructions. *Functional Plant Biology*, *29*(3), 323–333. https://doi.org/10.1071/pp01183

Lechno-Yossef, S., Rohnke, B. A., Belza, A. C. O., Melnicki, M. R., Montgomery, B. L., & Kerfeld, C. A. (2020). Cyanobacterial carboxysomes contain an unique rubisco-activase-like protein. *New Phytologist*, *225*(2), 793–806. https://doi.org/10.1111/nph.16195

Liang, F., & Lindblad, P. (2017). Synechocystis PCC 6803 overexpressing RuBisCO grow faster with increased photosynthesis. *Metabolic Engineering Communications*, *4*, 29–36. https://doi.org/10.1016/j.meteno.2017.02.002

Lloyd, M. K., McClelland, H. L. O., Antler, G., Bradley, A. S., Halevy, I., Junium, C. K., Wankel, S. D., & Zerkle, A. L. (2020). The isotopic imprint of life on an evolving planet. *Space Science Reviews*, *216*(7), 1–54. https://doi.org/10.1007/s11214-020-00730-6

Luo, X., Li, J., Chang, T., He, H., Zhao, Y., Yang, X., Zhao, Y., & Xu, Y. (2019). Stable reference gene selection for RT-qPCR analysis in Synechococcus elongatus PCC 7942 under abiotic stresses. *BioMed Research International*, *2019*, 7630601. https://doi.org/10.1155/2019/7630601

Lyons, T. W., Fike, D. A., & Zerkle, A. (2015). Emerging biogeochemical views of Earth's ancient microbial worlds. *Elements*, *11*(6), 415–421. https://doi.org/10.2113/gselements.11.6.415

Lyons, T. W., Reinhard, C. T., & Planavsky, N. J. (2014). The rise of oxygen in Earth's early ocean and atmosphere. *Nature*, *506*(7488), 307–315. https://doi.org/10.1038/nature13068

MacFarlane, J. J., & Raven, J. A. (1990). C, N and P nutrition of Lemanea mamillosa Kutz. (Batrachospermales, Rhodophyta) in the Dighty burn, Angus, U.K. *Plant, Cell and Environment*, *13*(1), 1–13. https://doi.org/10.1111/j.1365-3040.1990.tb01294.x

Maeda, S., Price, G. D., Badger, M. R., Enomoto, C., & Omata, T. (2000). Bicarbonate binding activity of the CmpA protein of the cyanobacterium *Synechococcus* sp. strain PCC 7942 involved in active transport of bicarbonate. *The Journal of Biological Chemistry*, *275*(27), 20551–20555. https://doi.org/10.1074/jbc.M003034200

Nisbet, E. G., Grassineau, N. V., Howe, C. J., Abell, P. I., Regelous, M., & Nisbet, R. E. R. (2007). The age of rubisco: The evolution of oxygenic photosynthesis. *Geobiology*, *5*, 311–335. https://doi.org/10.1111/j.1472-4669.2007.00127.x

Olson-Manning, C. F., Wagner, M. R., & Mitchell-Olds, T. (2012). Adaptive evolution: Evaluating empirical support for theoretical predictions. *Nature Reviews. Genetics*, *13*(12), 867–877. https://doi.org/10.1038/nrg3322

Omata, T., Gohta, S., Takahashi, Y., Harano, Y., & Maeda, S. (2001). Involvement of a CbbR homolog in low CO2-induced activation of the bicarbonate transporter operon in cyanobacteria. *Journal of Bacteriology*, *183*(6), 1891–1898. https://doi.org/10.1128/JB.183.6.1891-1898.2001

Onizuka, T., Akiyama, H., Endo, S., Kanai, S., Hirano, M., Tanaka, S., & Miyasaka, H. (2002). CO_2 response element and corresponding trans-acting factor of the promoter for Ribulose-1,5-bisphosphate carboxylase/oxygenase genes in *Synechococcus* sp. PCC7002 found by an improved electrophoretic mobility shift assay. *Plant and Cell Physiology*, *43*(6), 660–667. https://doi.org/10.1093/pcp/pcf082

Poudel, S., Pike, D. H., Raanan, H., Mancini, J. A., Nanda, V., Rickaby, R. E. M., & Falkowski, P. G. (2020). Biophysical analysis of the structural evolution of substrate specificity in RuBisCO. *Proceedings of the National Academy of Sciences*, *117*(48), 30451–30457. https://doi.org/10.1073/pnas.2018939117

Price, G. D., Badger, M. R., Woodger, F. J., & Long, B. M. (2008). Advances in understanding the cyanobacterial CO2-concentrating-mechanism (CCM): Functional components, ci transporters, diversity, genetic regulation and prospects for engineering into plants. *Journal of Experimental Botany*, *59*(7), 1441–1461. https://doi.org/10.1093/jxb/erm112

Rau, G. H., Riebesell, U., & Wolf-Gladrow, D. (1996). A model of photosynthetic ^{13}C fractionation by marine phytoplankton based on diffusive molecular CO_2 uptake. *Marine Ecology Progress Series*, *133*, 275–285. https://doi.org/10.3354/meps133275

Raven, J. A. (2013). Rubisco: Still the most abundant protein of earth? *New Phytologist*, *198*(1), 1–3. https://doi.org/10.1111/nph.12197

Raven, J. A., Cockell, C. S., & De La Rocha, C. L. (2008). The evolution of inorganic carbon concentrating mechanisms in photosynthesis. *Philosophical Transactions of the Royal Society, B: Biological Sciences*, *363*(1504), 2641–2650. https://doi.org/10.1098/rstb.2008.0020

Rillema, R., MacCready, J. S., & Vecchiarelli, A. G. (2020). Cyanobacterial growth and morphology are influenced by carboxysome positioning and temperature. https://doi.org/10.1101/2020.06.01.127845

Rippka, R., Deruelles, J., Waterbury, J. B., Herdman, M., & Stanier, R. Y. (1979). Generic assignments, strain histories and properties of pure cultures of cyanobacteria. *Microbiology*, *111*(1), 1–61. https://doi.org/10.1099/00221287-111-1-1

Roeske, C. A., & O'Leary, M. H. (1984). Carbon isotope effects on the enzyme-catalysed carboxylation of ribulose bisphosphate. *Biochemistry*, *23*, 6275–6284.

Schidlowski, M. (1988). A 3,800-million-year isotopic record of life from carbon in sedimentary-rocks. *Nature*, *333*(6171), 313–318. https://doi.org/10.1038/333313a0

Schidlowski, M. (2001). Carbon isotopes as biogeochemical recorders of life over 3.8 Ga of earth history: Evolution of a concept. *Precambrian Research*, *106*(1–2), 117–134. https://doi.org/10.1016/S0301-9268(00)00128-5

Schirrmeister, B. E., Sanchez-Baracaldo, P., & Wacey, D. (2016). Cyanobacterial evolution during the Precambrian. *International Journal of Astrobiology*, *15*(3), 187–204. https://doi.org/10.1017/s1473550415000579

Schopf, J. W. (2011). The paleobiological record of photosynthesis. *Photosynthesis Research*, *107*(1), 87–101. https://doi.org/10.1007/s11120-010-9577-1

Schubert, B. A., & Jahren, A. H. (2012). The effect of atmospheric CO_2 concentration on carbon isotope fractionation in C_3 land plants. *Geochimica et Cosmochimica Acta*, *96*, 29–43. https://doi.org/10.1016/j.gca.2012.08.003

Scott, K. M., Henn-Sax, M., Harmer, T. L., Longo, D. L., Frame, C. H., & Cavanaugh, C. M. (2007). Kinetic isotope effect and biochemical characterization of form IA RubisCO from the marine cyanobacterium *Prochlorococcus marinus* MIT9313. *Limnology and Oceanography*, *52*(5), 2199–2204.

Sengupta, A., Sunder, A. V., Sohoni, S. V., & Wangikar, P. P. (2019). Fine-tuning native promoters of Synechococcus elongatus PCC 7942 to develop a synthetic toolbox for heterologous protein expression. *ACS Synthetic Biology*, *8*(5), 1219–1223. https://doi.org/10.1021/acssynbio.9b00066

Smith, R. M., & Williams, S. B. (2006). Circadian rhythms in gene transcription imparted by chromosome compaction in the cyanobacterium *Synechococcus elongatus*. *Proceedings of the National Academy of Sciences*, *103*(22), 8564–8569. https://doi.org/10.1073/pnas.0508696103

Sprouffske, K., & Wagner, A. (2016). Growthcurver: An R package for obtaining interpretable metrics from microbial growth curves. *BMC Bioinformatics*, *17*, 172. https://doi.org/10.1186/s12859-016-1016-7

Stepien, C. C., & Austin, A. (2015). Impacts of geography, taxonomy and functional group on inorganic carbon use patterns in marine macrophytes. *Journal of Ecology*, *103*(6), 1372–1383. https://doi.org/10.1111/1365-2745.12451

Szekeres, E., Sicora, C., Dragos, N., & Druga, B. (2014). Selection of proper reference genes for the cyanobacterium Synechococcus PCC 7002 using real-time quantitative PCR. *FEMS Microbiology Letters*, *359*(1), 102–109. https://doi.org/10.1111/1574-6968.12574

Taton, A., Erikson, C., Yang, Y., Rubin, B. E., Rifkin, S. A., Golden, J. W., & Golden, S. S. (2020). The circadian clock and darkness control natural competence in cyanobacteria. *Nature Communications*, *11*(1), 1688. https://doi.org/10.1038/s41467-020-15384-9

Taton, A., Unglaub, F., Wright, N. E., Zeng, W. Y., Paz-Yepez, J., Brahamsha, B., Palenik, B., Peterson, T. C., Haerizadeh, F., Golden, S. S., & Golden, J. W. (2014). Broad-host-range vector system for synthetic biology and biotechnology in cyanobacteria. *The Nucleic Acids Research*, *42*(17), e136. https://doi.org/10.1093/nar/gku673

Taylor, T. B., Shepherd, M. J., Jackson, R. W., & Silby, M. W. (2022). Natural selection on crosstalk between gene regulatory networks facilitates bacterial adaptation to novel environments. *Current Opinion in Microbiology*, *67*, 102140. https://doi.org/10.1016/j.mib.2022.02.002

Tcherkez, G. G., Farquhar, G. D., & Andrews, T. J. (2006). Despite slow catalysis and confused substrate specificity, all ribulose bisphosphate carboxylases may be nearly perfectly optimized. *Proceedings of the National Academy of Sciences of the United States of America*, *103*(19), 7246–7251. https://doi.org/10.1073/pnas.0600605103

Tchernov, D., Helman, Y., Keren, N., Luz, B., Ohad, I., Reinhold, L., Ogawa, T., & Kaplan, A. (2001). Passive entry of CO2 and its energy-dependent intracellular conversion to HCO3- in cyanobacteria are driven by a photosystem I-generated deltamuH+. *The Journal of Biological Chemistry*, *276*(26), 23450–23455. https://doi.org/10.1074/jbc.M101973200

Ungerer, J., Lin, P.-C., Chen, H.-Y., Pakrasi, H. B., Giovannoni, S. J., Burnap, R., & Sherman, L. (2018). Adjustments to photosystem stoichiometry and electron transfer proteins are key to the remarkably fast growth of the cyanobacterium Synechococcus elongatus UTEX 2973. *MBio*, *9*(1), e02327-17. https://doi.org/10.1128/mBio.02327-17

Vijayan, V., Jain, I. H., & O'Shea, E. K. (2011). A high resolution map of a cyanobacterial transcriptome. *Genome Biology*, *12*(5), R47. https://doi.org/10.1186/gb-2011-12-5-r47

von Caemmerer, S., Tazoe, Y., Evans, J. R., & Whitney, S. M. (2014). Exploiting transplastomically modified rubisco to rapidly measure natural diversity in its carbon isotope discrimination using tuneable diode laser spectroscopy. *Journal of Experimental Botany*, *65*(13), 3759–3767. https://doi.org/10.1093/jxb/eru036

Wilhelm, S. W., Bullerjahn, G. S., McKay, R. M. L., & Moran, M. A. (2020). The complicated and confusing ecology of Microcystis blooms. *MBio*, *11*(3), e00529-20. https://doi.org/10.1128/mBio.00529-20

Wilkes, E. B., Lee, R. B. Y., McClelland, H. L. O., Rickaby, R. E. M., & Pearson, A. (2018). Carbon isotope ratios of coccolith–associated polysaccharides of *Emiliania huxleyi* as a function of growth rate and CO_2 concentration. *Organic Geochemistry*, *119*, 1–10. https://doi.org/10.1016/j.orggeochem.2018.02.006

Wilkes, E. B., & Pearson, A. (2019). A general model for carbon isotopes in red-lineage phytoplankton: Interplay between unidirectional processes and fractionation by RubisCO. *Geochimica et Cosmochimica Acta*, *265*, 163–181. https://doi.org/10.1016/j.gca.2019.08.043

Wilson, A. C., Maxson, L. R., & Sarich, V. M. (1974). Two types of molecular evolution. Evidence from studies of interspecific hybridization. *Proceedings of the National Academy of Sciences*, *71*(7), 2843–2847. https://doi.org/10.1073/pnas.71.7.2843

Wong, W. W., & Sackett, W. M. (1978). Fractionation of stable carbon isotopes by marine phytoplankton. *Geochimica et Cosmochimica Acta*, *42*(12), 1809–1815. https://doi.org/10.1016/0016-7037(78)90236-3

Yu, J., Liberton, M., Cliften, P. F., Head, R. D., Jacobs, J. M., Smith, R. D., Koppenaal, D. W., Brand, J. J., & Pakrasi, H. B. (2015). *Synechococcus elongatus* UTEX 2973, a fast growing cyanobacterial chassis for biosynthesis using light and CO2. *Scientific Reports*, *5*(1), 8132. https://doi.org/10.1038/srep08132

Yumol, L. M., Uchikawa, J., & Zeebe, R. E. (2020). Kinetic isotope effects during CO2 hydration: Experimental results for carbon and oxygen fractionation. *Geochimica et Cosmochimica Acta*, *279*, 189–203. https://doi.org/10.1016/j.gca.2020.03.041

Zavřel, T., Sinetova, M., & Červený, J. (2015). Measurement of chlorophyll *a* and carotenoids concentration in cyanobacteria. *Bio-Protocol*, *5*(9), e1467. https://doi.org/10.21769/BioProtoc.1467

SUPPORTING INFORMATION

Additional supporting information can be found online in the Supporting Information section at the end of this article.

How to cite this article: Garcia, A. K., Kędzior, M., Taton, A., Li, M., Young, J. N., & Kaçar, B. (2023). Effects of RuBisCO and CO_2 concentration on cyanobacterial growth and carbon isotope fractionation. *Geobiology*, *21*, 390–403. https://doi.org/10.1111/gbi.12543